INFLUENCE OF RESONANT MAGNETIC PERTURBATION ON FLOW AND TURBULENCE DYNAMICS TOWARDS L-H TRANSITION IN HL-3

[1]M. JIANG, [1]Y. ZHANG, [2]Z. B. GUO, [1]Z. B. Shi, [3]P. H. DIAMOND, [4]W. X. GUO, [1]J. Q. XU, [1]N. ZHANG, [1]Z. WANG, [1]Z. J. LI, [1]Y. ZHOU, [1]A. S. LIANG, [1]T. F. SUN, [1]R. KE, [1]S. B. GONG, [1]X. X. HE, [1]W. CHEN AND [1]W. L. ZHONG
[1]Southwestern Institute of Physics, Chengdu, China
[2]State Key Laboratory of Nuclear Physics and Technology, Fusion Simulation Center, School of Physics, Peking University, Beijing, China
[3]University of California San Diego, La Jolla, California, USA
[4]International Joint Research Laboratory of Magnetic Confinement Fusion and Plasma Physics, State Key Laboratory of Advanced Electromagnetic Engineering and Technology, School of Electric and Electronic Engineering, Huazhong University of Science and Technology, Wuhan, China

Abstract

The externally applied resonant magnetic perturbation (RMP) has been demonstrated to be an effective way to mitigate and suppress the edge localized modes in H-mode plasmas in present tokamaks. However, it was found recently in HL-3 tokamak, both n=1 and n=2 RMPs increase the L-H transition power threshold. Following the RMP application, the equilibrium flow shear in the edge region is substantially reduced. This reduction, combined with enhanced micro-instabilities driven by increased profile gradients, leads to enhanced turbulence levels. Consequently, the diminished flow shear becomes less effective in suppressing turbulence, providing a comprehensive explanation for the inhibited access to H-mode. Through a modified one-dimensional predator-prey model that incorporates the effects of RMP-induced radial magnetic perturbations, we have conducted a quantitative analysis of the turbulence and flow dynamics during the L-H transition process. Our results indicate that as the strength of magnetic perturbation increases, the turbulence intensity increases and edge flow shear decreases, in agreement with experimental observations. These results enhance our understanding of RMP-induced changes in edge plasma transport, providing valuable insights for optimizing the operation of future tokamaks and improving the performance of fusion reactors.

1. INTRODUCTION

Resonant magnetic perturbation has emerged as an effective technique for mitigating or suppressing ELMs, thereby protecting plasma-facing components and managing the heat load on the divertor [1, 2, 3]. To prevent the occurrence of the first large ELM, it may be necessary to apply RMP before the L-H transition. However, the application of RMP in L-mode plasmas has been observed to increase the L-H transition power threshold（P_{LH}）on JFT-2M [4], MAST [5], NSTX [6], DIII-D [7], ASDEX-Upgrade [8] and KSTAR [9], which may inhibit access to H-mode and present operational challenges for next-generation tokamaks. This increase in P_{LH} is particularly concerning for ITER, where the available auxiliary heating power may only marginally exceed the predicted P_{LH} without considering the effects of RMP [10, 11].

The impact of RMP on the L-H transition is a complex issue involving the interplay between plasma turbulence, flows, and the applied magnetic perturbations. Experimental investigations on the DIII-D tokamak have revealed that the n=3 RMP can reduce flow shearing rates and increase turbulence decorrelation rates [12, 13], disrupting the turbulence suppression mechanism that is essential for the L-H transition [14]. Additionally, RMP has been found to decrease the rate of Reynolds-stress-driven energy transfer from turbulence to flows during the L-H transition, challenging the energy depletion theory for the L-H trigger mechanism [13]. Experimental results on ASDEX-Upgrade and KSTAR indicate that L-H transition threshold power increases only when the perturbed magnetic field strength is above a critical value [9, 15].

In this work, we present a detailed analysis of the effects of n = 1 RMP on the L-H transition on the HL-3 tokamak. We investigate how RMP alters the equilibrium profiles and turbulence-flow characteristics in the stationary L-mode state preceding the L-H transition. Furthermore, we introduce a modified one-dimensional predator-prey model that incorporates the effects of RMP to quantitatively study the turbulence-flow dynamics and the dependence of the L-H transition power threshold on radial magnetic perturbation intensity.

2. POWER THRESHOLD INCREASED BY N=1 AND N=2 RMP

The experiments were conducted with a plasma current Ip = 0.5 MA, toroidal magnetic field Bt = 1.5 T, and edge safety factor $q_{95}\approx 5$. Figure 1 shows the changes of the L-H transition power threshold with the relative radial magnetic field strength ($\delta B_r/B$) produced by RMPs. It is found that for both n=1 and n=2 RMPs the P_{LH} increases with the magnetic field strength when it is above a threshold, consistent with the observations on ASDEX-Upgrade and KSTAR [9, 15]. The $\delta B_r/B$ threshold is relevant to the plasma response to the applied RMP. In addition, for n=2 RMP, the $\delta B_r/B$ threshold seems to be larger than that of n=1 RMP, since the plasma still sustains in L-mode phase with the heating power of 2.3 MW as denoted by the blue circle in figure 1.

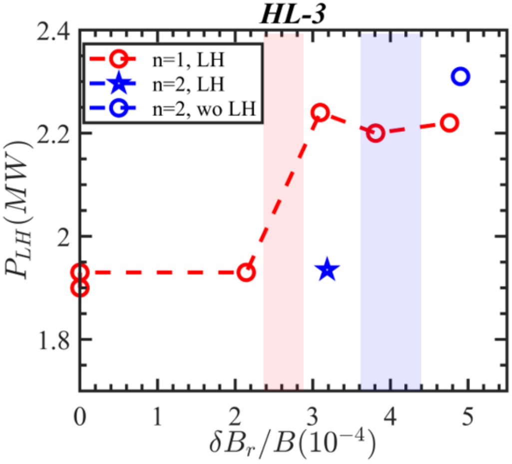

Figure 1. L-H transition power threshold versus the relative radial magnetic field strength ($\delta B_r/B$) produced by n=1 and n=2 RMPs.

3. OBSERVATION OF L-H TRANSITION INHIBITED BY THE RMP

Figure 2 presents a comparative analysis of the typical discharge parameters for two HL-3 shots, 6550 and 6553, under similar experimental conditions. In shot 6550, no RMP was applied, and the L-H transition occurred at t =1723.5ms, as indicated by the red vertical dashed line in figure 2. Following the transition, ELMs appeared, characterized by typical D_α intensity spikes. Based on the final two steps of the NBI heating power, it can be inferred that the L-H transition power threshold P_{LH} lies between 1.25 MW and 1.8 MW. P_{LH} is calculated as the sum of the NBI power P_{NBI}, ECRH power P_{ECRH}, and Ohmic power P_{OH} (0.2MW), minus the change in stored energy dWe/dt (0.25MW): $P_{LH} = P_{NBI} + P_{ECRH} + P_{OH} - dWe/dt$. This aligns well with the Martin08 scaling law [10], which estimated that the L-H transition power threshold to be approximately 1.3 MW.

In contrast, in shot 6553, the RMP was activated at t = 1100ms with a constant current I_{RMP} = 6.5kAt. Figure 2(d) shows that after the RMP was turned on, the D^α intensity was higher than that in shot 6550, indicating enhanced transport due to the RMP. Notably, no L-H transition occurred around t = 1723.5ms in shot 6553, and the system remained in L-mode throughout the experiment. The inhibition of H-mode access due to strong RMP field has been also observed on DIII-D [7] and MAST [5].

4. CHANGES OF EQUILIBRIUM FLOW-TURBULENCE DYNAMICS BY RMPS

To understand why the RMP inhibited the L-H transition, we compared the equilibrium profiles at the time slice of t = 1722ms (L-mode state), just before the L-H transition in shot 6550. In the presence of RMP, the outer region ($0.385 < \rho < 1$) exhibited higher density, while the inner region ($0 < \rho < 0.385$) showed lower density (not shown here). For the percent difference comparison with the no RMP case, we found that in the application of RMP, the electron temperature profile drops by 45% in the radial range of $0.85 < \rho < 1$, and drops by 21% in the range of $0.15 < \rho < 0.75$. The ion temperature also decreased across the entire radial profile, while the toroidal rotation did not change significantly.

The modification of the equilibrium profiles potentially alters the essential factor affecting the L-H transition process, i.e., the $E_r \times B$ velocity, particularly the associated velocity shear. In experiments, the DBS measures $V_\perp$ by detecting the sum of the $E_r \times B$ drift velocity and the turbulence phase velocity. Typically, in Ohmic or L-mode discharges, the $E_r \times B$ velocity dominates over the turbulent component, making the measured velocity primarily reflect the $E_r \times B$ drift velocity. It should be mentioned that at the lower wavenumber range covered by DBS (e.g. $k_y \rho_s$ = 0.4, where k_y is the poloidal wave number and ρ_s is the ion sound Lamor radius), the phase velocity may not be negligible. The precise definition for '⊥' is the velocity perpendicular to the helical magnetic field lines. Figure 3 shows the measured perpendicular velocity $V_\perp$ profile using the DBS diagnostics, where the markers with error bars represent the experimental data points, and the solid lines of the same color represent the corresponding fitting profiles. The relative distance between $V_\perp$ well minimum and last closed flux surface is about 6-7 cm in HL-3 real space, which is larger than that observed in other machines [12, 15]. This maybe resulted from the relatively broad equilibrium profiles in HL-3. Without RMP, $V_\perp$ is negative in the edge region, and a well developed E_r well (where $E_r \approx V_\perp B$) was observed (red markers and curve in Fig. 3(a)), characterized by large E_r-shear ($V'_{\perp,\rho=0.93} \sim$ 84 kHz, red curve in figure 3(b)). With RMP applied, the 'U' shape $V_\perp$ becomes broader (blue markers and curve in Fig.3(a)) with a similar depth but the velocity shear decreased by about 57% ($V'_{\perp,\rho=0.93} \sim$36 kHz) around the radial location of ρ=0.93 (blue curve in figure 3(b)). On DIII-D, with the application of RMP, the depth of $E_r \times B$ flow profile decreased or even reversed sign at high RMP strength, while the width stayed roughly constant, leading a reduction of $E_r \times B$ velocity shear [18]. Fundamentally, the reduction in the L-mode $E_r \times B$ velocity shear induced by the n=1 RMP on HL-3 mirrors the effects observed on DIII-D with n=3 RMP [12]. This similarity of reduced $E_r \times B$ velocity shear highlights the consistent impact of RMP on plasma flow dynamics across different tokamaks and toroidal mode numbers.

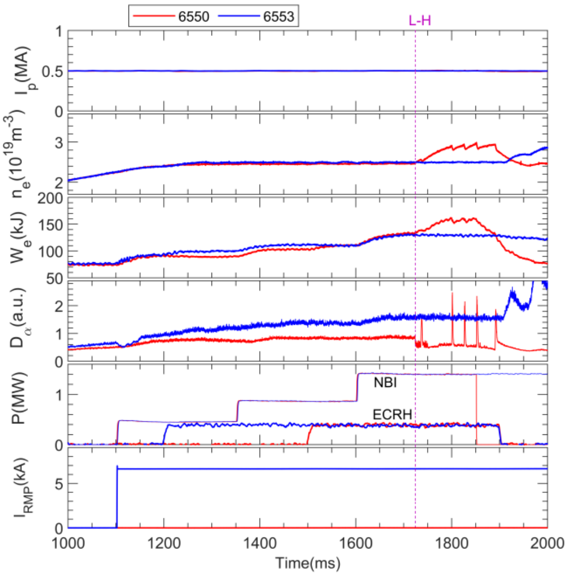

Figure 2. Time evolutions of the discharge parameters in shot 6550 and 6553, with (a) the plasma current I_p, (b) the line-averaged electron density n_e, (c) the stored energy W_e, (d) the D_α intensity in the divertor, (e) the NBI and ECRH heating power, and (f) the RMP current I_{RMP}. The red vertical dashed line marks the L-H transition time in shot 6550.

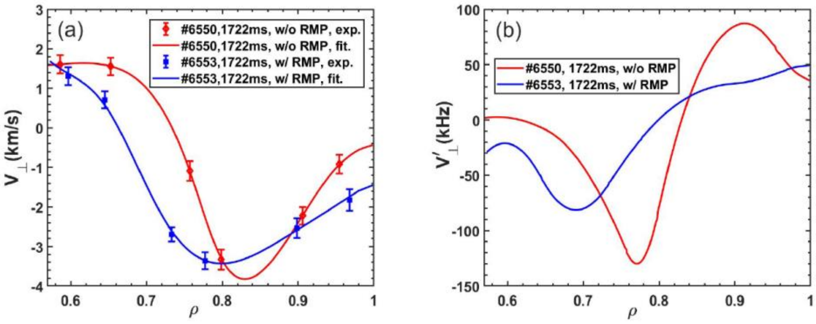

Figure 3. (a) Perpendicular velocity $\boldsymbol{V}_{\perp}$ *measured by the DBS diagnostics, where the markers with error bars represent the measured experimental data points and the solid lines with the same color represent the corresponding fitting profiles, respectively. (b) Velocity shear calculated from the fitting profiles in (a).*

Apart from the macro-scale quantities, we also investigated how RMP affects the turbulence behaviors. The data points averaged over a 0.5 ms time window from 1721 ms to 1723 ms (centered at 1722 ms) were used for the DBS and BES measurements. To get rid of the impact of large scale MHD perturbations, we chose to consider frequency range above 10 kHz for turbulence comparison. The radial distribution of experimentally measured density perturbations, as shown in figure 4(a), indicating that the presence of RMP leads to higher turbulence intensity compared to the case without RMPs. In addition, we calculated the auto-correlation time of the density perturbations using both BES and DBS diagnostics, as shown in figure 4(b). The results indicate that, regardless of whether the frequency band is low (10–60 kHz) or high (200–350 kHz), the auto-correlation time remains nearly unchanged. Specifically, the auto-correlation time is approximately 5 μs for the low-frequency band and 1 μs for the high-frequency band, respectively. It should be mentioned that the auto-correlation time could be used as a measure of the turbulence correlation time. However, the auto-correlation time also depends on the turbulence correlation length and velocity. If the turbulence velocity is large enough, then the auto-correlation time could be substantially smaller than the true turbulence correlation time. This may mask changes in the turbulence correlation time caused by the RMP. The slight reduction in auto-correlation time with RMP at the outermost radius (ρ>0.9) is qualitatively consistent with the larger E_r × B velocity measured by DBS in this region (figure 3(a)).

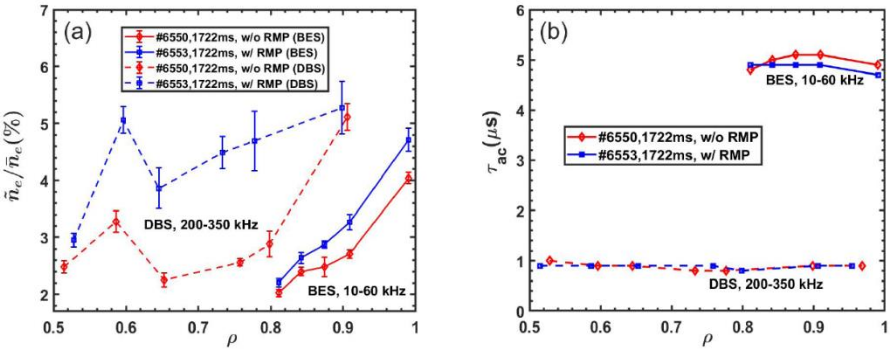

Figure 4. (a) Amplitude of electron density perturbation $\tilde{n}_e/\bar{n}_e$ *in the range of 10–60 kHz measured by the BES diagnostics (solid curves) and 200–350 kHz measured by the DBS diagnostics (dashed curves). The error bars in the figure were estimated by statistical standard deviations during 1721–1723 ms. (b) Auto-correlation time of the density perturbation with the low-frequency band (10–60 kHz) measured by the BES and high-frequency and (200–350 kHz) measured by the DBS diagnostics.*

Since the equilibrium profiles were significantly altered by the RMP, the driving forces for instabilities, particularly through profile gradients changed accordingly. Based on the experimental parameters at the q=4 rational surface (ρ=0.876), we performed gyrokinetic simulations using the GENE code [16] to compare the underlying turbulence intensities. It is found that the linear growth rate for shot 6553 was larger than that for shot 6550 across a broad range of normalized wave numbers, as shown in figure 5(a). Additionally, in both shots, the sign of the mode frequency reversed with increasing $k_y\rho_s$, transitioning from the electron diamagnetic drift direction to ion diamagnetic drift direction (figure 5(b)). This phenomenon is similar to a transition from trapped electron mode (TEM) with low wavenumber to the ubiquitous mode (UM) with high wavenumber [17].

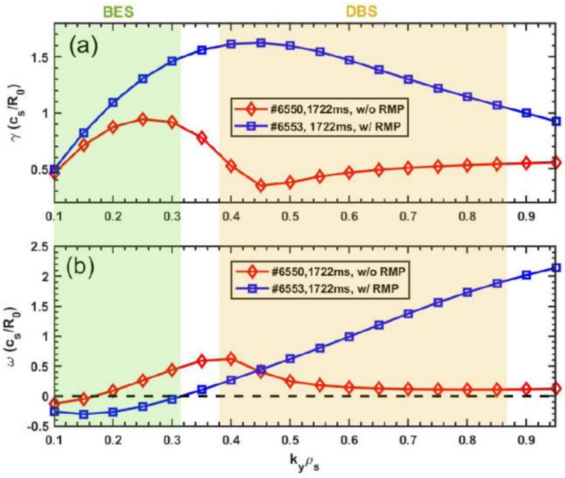

Figure 5. GENE simulations of the normalized (a) linear growth rates and (b) frequency of the unstable modes using experimental parameters at $\rho=0.875$, where c_s is the ion sound speed, k_y is the poloidal wavenumber and ρ_s is the ion sound Lamor radius. Positive (negative) frequencies in (b) stand for the ion (electron) diamagnetic drift direction. The green (yellow) shaded area indicates the wavenumber coverage of BES (DBS) measurements in experiments.

To quantify how RMP affected turbulence suppression by shear flow, we compared the effective shearing rate $\omega_{E\times B}$ with the turbulence decorrelation rate ω_D. Here $\omega_{E\times B}$ is defined as the Hahm–Burrell E×B shearing rate[1819]. The turbulence decorrelation rate is estimated from the reciprocal of auto-correlation time, i.e. $\omega_D = 1/\tau_{ac}$. As such, turbulence suppression by shear flow is characterized by the ratio between the effective shearing rate and decorrelation rate, i.e. $\omega_{E\times B}/\omega_D$. Since the E×B shear is more effective on large scale turbulence suppression, the actual decorrelation rate is calculated from the auto-correlation time measured by the BES diagnostic (i.e. $\tau_{ac} \sim 5\mu s$ in figure 4(b)). Figure 6 illustrates how RMP affected the shear suppression parameter $\omega_{E\times B}/\omega_D$. Without RMP, $\omega_{E\times B}/\omega_D$ is close to 1 in the edge region ($0.85 < \rho < 1$), with some values slightly larger than 1 ($\rho \sim 0.93$). This indicates that any mechanism driving additional shear flow, even transiently, would further suppress turbulence and trigger the L-H transition (red curves in figure 2). However, with RMP, $\omega_{E\times B}/\omega_D$ decreases significantly (below 0.7) throughout the whole edge region, implying that E×B shear flow has a weak suppression effect on the turbulence. As a result, more transient turbulence suppression and mean flow shear are required to trigger the L-H transition, necessitating higher heating power. This makes transitioning to H-mode more difficult and is consistent with the failure to enter H-mode as shown in figure 2 (blue curves). These results demonstrate that RMP disrupts the turbulence-shear suppression mechanism in the stationary L-mode state preceding the L-H transition.

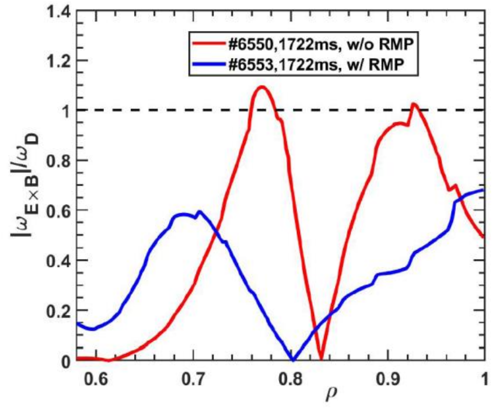

Figure 6. Turbulence suppression parameter $\omega_{E\times B}/\omega_D$ for the BES measured low-frequency density perturbation (10–60 kHz). The horizontal dashed line marks $\omega_{E\times B}/\omega_D = 1$, below which the shear flow could not adequately suppress the ambient turbulence.

5. ONE DIMENSIONAL PREDATOR–PREY SIMULATION IN THE PRESENCE OF MAGNETIC PERTURBATION

To study the L-H transition dynamics numerically, we extended the 5-field reduced mesoscale 1D predator–prey model to incorporate the effect of RMP, by combining the previous 1D L-H transition model without magnetic perturbation [20] and the effect of a uniform magnetic perturbation on the evolution of the zonal flow

[21, 22]. The effects of magnetic perturbations induced by RMP are modelled as stochastic dephasing relative to the turbulent decorrelation, as shown in [22]. Hence, a factor of $1/(1+\alpha)$ is introduced in the evolution equations for turbulence and zonal flow, representing the stochastic effect of Reynolds stress decoherence, where $\alpha = q\tilde{b}_r^2/(\sqrt{\beta}\rho_*^2\epsilon)$, with q, $\tilde{b}_r^2$, β, ρ*, ϵ being the safety factor, normalized radial magnetic perturbation induced by the RMP, the ratio of plasma pressure to the magnetic pressure, normalized gyro-radius and normalized density scale length, respectively. The details of the models can be found in reference [23].

All parameters are fixed but the α is scanned linearly to quantitatively explore the effects of RMP induced magnetic perturbation on the L-H transition dynamics as well as L-H transition power threshold. Figures 7(a)–(c) present the spatiotemporal evolution of turbulence intensity I, mean square zonal flow shear E_{ZF}, and mean E×B flow shear E_V for the case without RMP (α=0.0), which illustrate that a standard L-H transition occurs through limit-cycle-oscillation (LCO). Initially, the plasma is in the L-mode state ($0 < t < 2.1\times10^5$, $Q_{max} = 5\times10^{-4}$), characterized by low heating power and slow growth of turbulence, which is self-regulated by the zonal flow. The mean flow shear is weak, and the interaction between zonal flow and mean flow is not significant. As the heating power increases linearly from $Q_{max} = 5\times10^{-4}$ to $Q_{max} = 2\times10^{-2}$ during $2.1\times10^5 < t < 2.6\times10^5$, the system evolves into the I-phase with LCO, characterized by strong oscillations of edge turbulence, zonal flow and mean flow shear, along with inward propagating waves. When the heating power Q_{max} exceeds a critical value of 0.0101 ($t = 2.346\times10^5$), the LCO abruptly terminates, leading to a rapid quench of edge turbulence and zonal flow. This marks the onset of the L-H transition, where an ETB forms as the mean flow shear rapidly increases. After the L-H transition, the pedestal width of the ETB quickly saturates, even though the heating power continues to increase. A steady H-mode state persists in the late stages of the simulation.

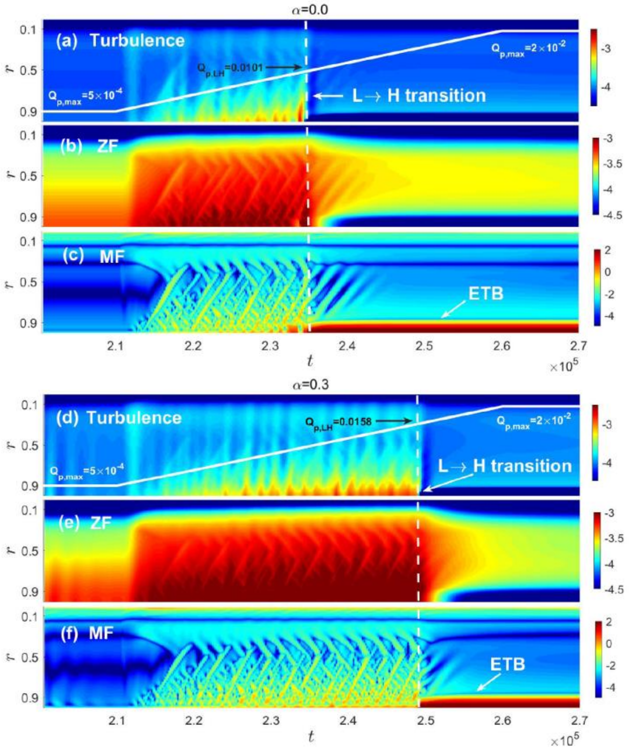

Figure 7. Spatiotemporal evolution of turbulence intensity log$_{10}$*I, Zonal flow log*$_{10}$*E*$_{ZF}$ *and mean flow log*$_{10}$*E*$_V$ *in the cases of α=0 and α=0.3. The vertical white dashed lines mark the L-H transition time.*

In contrast, figures 7(d)–(f) show the same quantities for the case with RMP (α=0.3). For the same heating procedure, the LCO stage lasts longer, extending from $t = 2.1\times10^5$ to $t = 2.492\times10^5$. Only when the heating power reaches $Q_{max} = 0.0158$ does the L-H transition occur, followed by the formation of the ETB and entry into a steady H-mode state. Comparing the two cases, it is evident that the presence of RMP delays the L-H transition, requiring more heating power to achieve L-H transition. Specifically, if the heating power only grows to $Q_{max} = 0.0101$, the L-H transition is inhibited by the RMP. This phenomenon is consistent with the experimental findings on HL-3 tokamak as shown in figure 2.

To further understand the mechanisms behind this delay, we compared the radial profiles during the LCO state at $t = 2.3\times10^5$ between the cases of α=0 and α=0.3. Figure 8 shows that, compared to the no RMP case (α=0), the presence of RMP (α=0.3) leads to increased turbulence intensity (figure 8(a)), enhanced zonal flow shear (figure 8(b)), strong reduction of poloidal mass flow in the edge region (figure 8(c)), nearly unchanged density (figure 8(d)), reduced temperature and pressure in the core region (but remain nearly the same in the edge region, (figures 8(e)–(f)), and significant decrease in edge mean flow shear (figure 8(g)). The reduction in mean flow shear is particularly important because it weakens the turbulence suppression mechanism. As a result, more heating power is required to replenish the mean flow shear and trigger the L-H transition. This explains why the L-H transition is delayed in the presence of RMP. The decreased mean flow shear caused by RMP shares similar features to the experimental findings on HL-3 tokamak.

Figure 9 shows that as α increases, the L-H transition threshold heating power Q_{LH} increases accordingly. Specifically, we found that Q_{LH} almost linearly increases with the square of the strength of magnetic perturbation α, with a fitting formula of $Q_{LH} = 0.02\times\alpha+Q_{LH,\mathrm{w/o\ RMP}}$, where $Q_{LH,\mathrm{w/o\ RMP}}$ is the power threshold without RMP. Even though the case of α=0.2 appears to slightly deviate from the main trend, the turbulence-flow-gradient dynamics is nearly the same as other cases. The observed threshold heating power dependence on the magnitude of magnetic perturbations is consistent with the theoretical predictions [22] as well as the 0 D modified predator–prey model of the L-H transition with stochastic fields included [21]. We found that the trend of the L-H transition power threshold also increases with α even though we change the input parameter with a faster heating scheme, e.g. the heating power increases linearly from $Q_{max} = 5\times10^{-4}$ to $Q_{max} = 2\times10^{-2}$ during $2.1\times10^{5} < t < 2.3\times10^{5}$.

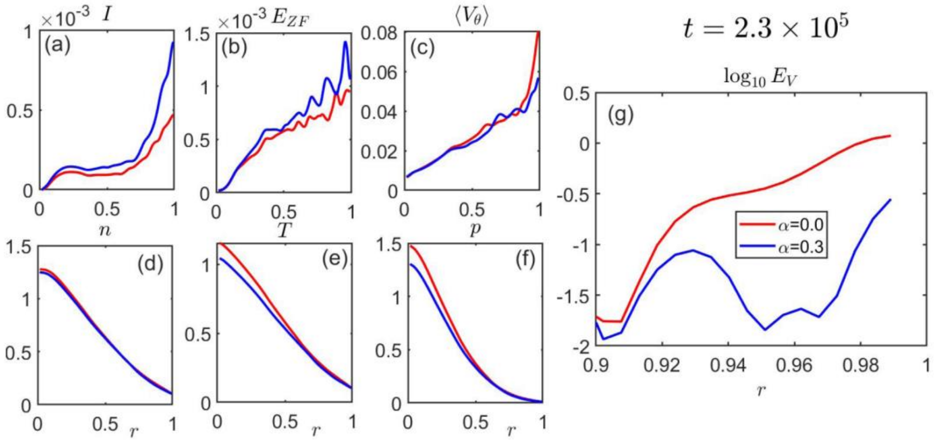

Figure 8. Radial profiles before the L-H transition, i.e. LCO state at $t = 2.3\times10^{5}$: (a) turbulence intensity I, (b) zonal flow shear E_{ZF}, (c) poloidal mass flow $\langle V_\theta\rangle$, (d) density n, (e) temperature T, (f) pressure p and (g) mean flow shear E_V.

6. SUMMARY

The dedicated experiments conducted on the HL-3 tokamak have provided comprehensive insights into the effects of n=1 RMP on the L-H transition. A notable reduction in equilibrium flow shear and an increase in turbulence intensity were observed, which are pivotal in influencing the L-H transition threshold. These alterations in plasma dynamics weaken the turbulence suppression mechanism, making it more difficult to achieve the conditions necessary for the L-H transition. A modified 1D predator–prey model that incorporates the influence of RMP-induced magnetic perturbations has been developed and employed to gain a deeper understanding of these effects. It is found that the L-H transition power threshold exhibits an approximately linear relationship with the square of the radial magnetic perturbation intensity. This quantitative analysis underscores the critical role of RMP in modifying the plasma's behavior during the L-H transition. These findings highlight the necessity for a better understanding of RMP-induced changes in plasma behavior, which is crucial for optimizing the operational parameters of tokamaks and enhancing the performance of future fusion reactors.

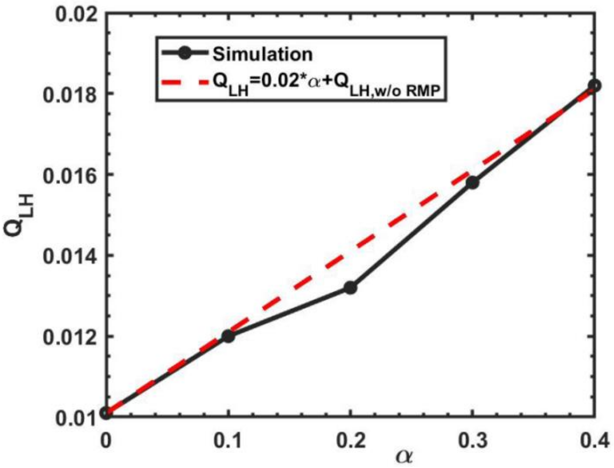

Figure 9. L-H transition power threshold QLH respective to the square of the strength of radial magnetic perturbation α. The black circles represent simulation results and the red dashed line represents fitting result.

ACKNOWLEDGEMENTS

This project was supported by the National MCF Energy R&D Program (Nos. 2022YFE03060003 and 2024YFE03270400), the National Natural Science Foundation of China (Nos. 12075079, 12405256 and 12075013) and the Innovation Program of Southwestern Institute of Physics (No. 202301XWCX001-02).

REFERENCES

[1] Evans T E et al., Phys. Rev. Lett. 92 235003 (2004).
[2] Jeon Y M et al., Phys. Rev. Lett. 109 035004 (2012).
[3] Sun Y et al., Phys. Rev. Lett. 117 115001 (2016).
[4] Leonard A et al., Nuclear Fusion 31 1511 (1991).
[5] Kirk A et al., Plasma Physics and Controlled Fusion 53 065011 (2011).
[6] Kaye S et al., Nuclear Fusion 51 113019 (2011).
[7] Gohil P et al., Nuclear Fusion 51 103020 (2011).
[8] Ryter F et al., Nuclear Fusion 52 114014 (2012)
[9] In Y et al., Nuclear Fusion 57 116054 (2017).
[10] Martin Y R et al., Journal of Physics: Conference Series 123 012033 (2008).
[11] DJ Campbell A Loarte D B et al. ITER Research Plan within the Staged Approach (ITER Organization) (2024)
[12] Schmitz L et al., Nuclear Fusion 59 126010 (2019).
[13] Kriete D M et al., Physics of Plasmas 27 062507 (2020).
[14] Yan Z et al., Phys. Rev. Lett. 112(12) 125002 (2014).
[15] Willensdorfer M et al., Physics of Plasmas 29 032506 (2022).
[16] Jenko F., Dorland W., Kotschenreuther M. and Rogers B.N. Phys. Plasmas 7 1904–10 (2000).
[17] Shen Y., Dong J., Li J., Han M., Li J., Sun A. and Qu H. Nucl. Fusion 59 106011 (2019).
[18] Hahm T.S. and Burrell K.H. Phys. Plasmas 2 1648–51 (1995).
[19] Burrell K.H. Phys. Plasmas 4 1499–518 (1997).
[20] Miki K., Diamond P.H., Gurcan O.D., Tynan G.R., Estrada T., Schmitz L. and Xu G.S. Phys. Plasmas 19 092306 (2012).
[21] Chen C.-C., Diamond P.H., Singh R. and Tobias S.M. Phys. Plasmas 28 042301 (2021).
[22] Li X., Guo Z. and Diamond P.H. Nucl. Fusion 64 044001 (2024)
[23] Y. Zhang et al Nucl. Fusion 65 066016 (2025).